Malaysian Journal of Chemistry, 2022, Vol. 24(1), 36-53

Fabrication and Characterization of Molybdenum Trioxide Nanoparticles and their Anticancer, Antibacterial and Antifungal Activities

Jayanti Kumari* and Preeti Mangala
Research Centre, Department of Chemistry, Jyoti Nivas College Autonomous, Bangalore University, Bangalore, Karnataka, India
*Corresponding author (e-mail: jayantikumari.dei@gmail.com)

The present study focused on the fabrication of molybdenum trioxide nanoparticles (MoO_3) from a molybdenum complex with *N*-salicylideneaniline [$Mo(C_{13}H_{10}NO)_3$] ligand as the precursor. The ligand was synthesized and characterized by ^1H NMR and ^{13}C NMR. The synthesized MoO_3 nanoparticles were characterized by *powder X-ray diffraction*, FT-IR, UV-visible spectroscopy, TG-DTA, SEM-EDX and TEM. The results clearly showed the formation of nanoparticles of MoO_3. The absorption spectra of MoO_3 at 341 nm revealed the formation of MoO_3 by calculating the band gap at 2.8 eV. TG–DTA showed MoO_3 was stable up to 800 °C. SEM and TEM analyses clearly indicated the formation of MoO_3 nanoparticles in the range of 30-47 nm. The NPs were tested for their cytotoxicity influence on MCF7-human breast adenocarcinoma cell lines. The findings suggested MoO_3 had the capacity to kill 50% of viable cells after 24 h of incubation at 37 °C. The observations strongly suggest that MoO_3 nanoparticles have therapeutic potential against human breast cancer cells based on the dosage of the drug after an incubation period of 24 h.

Key words: Molybdenum trioxide nanoparticles; efficient cancer therapy; biological activity; FT-IR; TGA; TEM

Received: October 2021; Accepted: December 2021

Cancer is a prevalent disease worldwide and kills more than 1500 people every day in the United States, according to the American Cancer Society (ACS, 2012) [1]. Researchers are exploring novel alternatives for cancer therapy. Nanomaterials have shown significant potential for the treatment of cancer due to their ability to overcome cell motility issues over the last decade [2-4]. Nanomaterials are emerging as an alternative to conventional chemotherapy due to their selective toxicity. The toxicity of nanoparticles (NPs) toward cancer cells depends on several elements, such as the size, shape and surface chemistry of the NPs, the specific cellular systems and the interactions among them [5]. Nanomaterial-assisted cancer therapy includes the controlled delivery of drugs/photosensitizers to reduce the side effects of chemo/photodynamic therapy [6], targeted drug delivery to kill specific cancer cells [7], magnetic hyperthermia [8], nano cryosurgery [9], sonodynamic therapy [10] and photothermal therapy [11]. Fundamental research involves the development of novel materials and the study of their toxicity toward cancer cells and the mode of cell death. This will lead to the development of materials for basic research in the biological sciences and clinical medicine [12,13]. The characteristics of nanomaterials are completely different as the behaviour and interactions of atoms are unique. The properties of atoms at the nano scale differ from the properties of bulk materials [14]. Molybdenum oxide nanomaterial shows antimicrobial activity. This can be attributed to its small size and high surface area to volume ratio which allows the particles to attach closely to the microbial membrane and release the metal ion in solution [15]. Bacteria, primarily *Staphylococcus aureus*, are a major cause of infections globally, from skin and soft tissue infections to more critical illnesses such as bacteremia, pneumonia, osteomyelitis, and endocarditis. The high morbidity and mortality correlated to *S. aureus* contamination is mainly due to its methicillin-resistant form (MRSA) [16]. This was historically linked to hospital-acquired infections, but eventually spread to the community. *S. aureus* can survive on a variety of environmental surfaces at a broad range of temperatures and humidity, even in sunlight [17]. Therefore, although transmission of *S. aureus* mainly occurs by direct human-to-human skin contact, environmental surfaces represent an important reservoir for dissemination as well. The death rate from fungal-related infections is also worrisome, and in a population of immune-compromised individuals, fungal infections can contribute toward an increase in morbidity and mortality rates [18]. Candida is a yeast that maintains a commensal relationship with the human body under

normal circumstances but in a situation where an individual has a compromised immune system, it becomes pathogenic [19, 20].

Nanoparticles (NPs) are worthy alternatives in combating fungal resistance to antifungal agents. The use of metal and metal oxide nanomaterials in cancer therapy has recently been investigated. The cytotoxic effects of silver and gold NPs on various cancer cell types have also been explored. Similarly, metal oxides such as ZnO, TiO_2, CeO_2, and CuO show selective toxicity toward cancer cells. The increasing death rates due to cancer and the failure and side effects of chemotherapeutic drugs have motivated researchers to develop new nanomaterials for cancer therapy [21-23]. In this regard, interest has focused on molybdenum trioxide (MoO_3) nanostructures because of their multifunctional properties in photocatalysis, electrochemical capacitors, oxidative catalysts and in antibacterial applications [24-26]. Molybdenum is an essential trace element for humans, animals, and plants. Molybdenum in trace concentrations can be found in foods such as cereal grains, cheese, leafy vegetables, legumes, milk, nuts, and organ meat. In the human body, molybdenum is stored in the bones, glands, liver, and kidneys [27]. It can also be located in the lungs, muscles, skin, and spleen, but almost 90% of molybdenum food is removed through urine. Medical applications of molybdenum are numerous, and include the prevention of dental caries, curing anaemia, enhancement of immunological reactions, and as an anticancer and antidiabetic agent [28-30]. Molybdenum has an antagonistic action against copper where high concentrations of molybdenum can decrease copper absorption and lead to copper deficiency. Hussain et al. demonstrated that MoO_3 NPs are less toxic than silver NPs against BRL 3A rat liver cells [31]. Stolle et al. showed that MoO_3 is less toxic than Ag NPs against a mouse spermatogonial stem cell line [32]. Recent studies of polyoxomolybdates (a structure containing discrete molybdenum oxide anion clusters) showed their potential antitumour activity toward pancreatic and gastric cancer cells [33]. Although many applications of MoO_3 NPs in various forms have been studied in biological systems in the past decade, few studies have examined the anticancer effects of nano MoO_3 on cancer cells. Hence, a study on the toxicity of MoO_3 nanomaterials towards cancer cells, as well as its antimicrobial and antifungal activities, would be of immense interest. Therefore, this study focussed on the cytotoxicity of MoO_3 nanomaterials on MCF-7 human breast adenocarcinoma cancer cell lines.

EXPERIMENTAL SECTION

1. Materials and Methods

All chemicals and reagents, purchased from Merck and Sigma-Aldrich, were analytical grade and used without any further purification.

2. Preparation of *N*-salicylideneaniline ($C_{13}H_{11}NO$) Ligand

Salicylaldehyde (1.22 g, 10 mmol) in methanol (10 mL) was added dropwise to a solution of aniline (1.22 g, 13.7 mmol) in methanol (10 mL). The mixture was stirred at 27 °C (room temperature) for 5 h. The solvent was allowed to evaporate and the yellow colour precipitate obtained was filtered and dried. The progress of the reaction was monitored by thin layer chromatography (TLC). The crude product was recrystallized with ethyl acetate (yield: 2.08 g, Scheme 1) [34].

3. Preparation of Molybdenum Trioxide Nanoparticles

Molybdenum trioxide nanoparticles (MoO_3) were synthesized from molybdenum *N*-salicylideneaniline complex [$Mo(C_{13}H_{10}NO)_3$] as precursor. 0.5 g molybdic acid (H_2MoO_4) and 2.0 g *N*-salicylideneaniline ($C_{13}H_{11}NO$) were added to ethanol (30 mL) and the reaction was allowed to run for 5 h with continuous stirring at 40 °C. The product was dried at room temperature for 6 days. The yield was found to be 2.175 g. The complex was ashed in a muffle furnace at 600 °C for 4 h and then weighed again. The yield after calcination was found to be 0.447 g (Scheme 2). This was characterized as molybdenum trioxide nanoparticles (MoO_3).

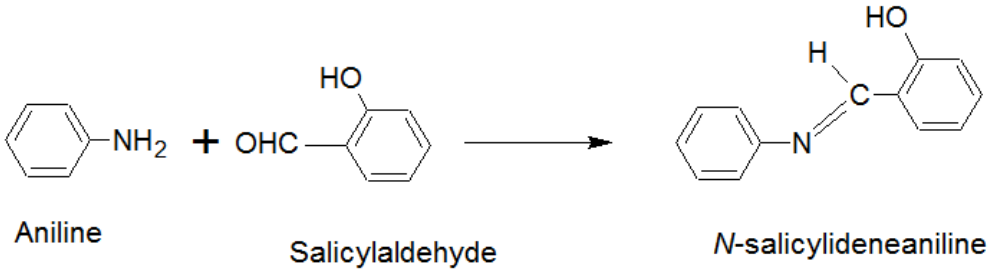

Scheme 1. Preparation of *N*-salicylideneaniline

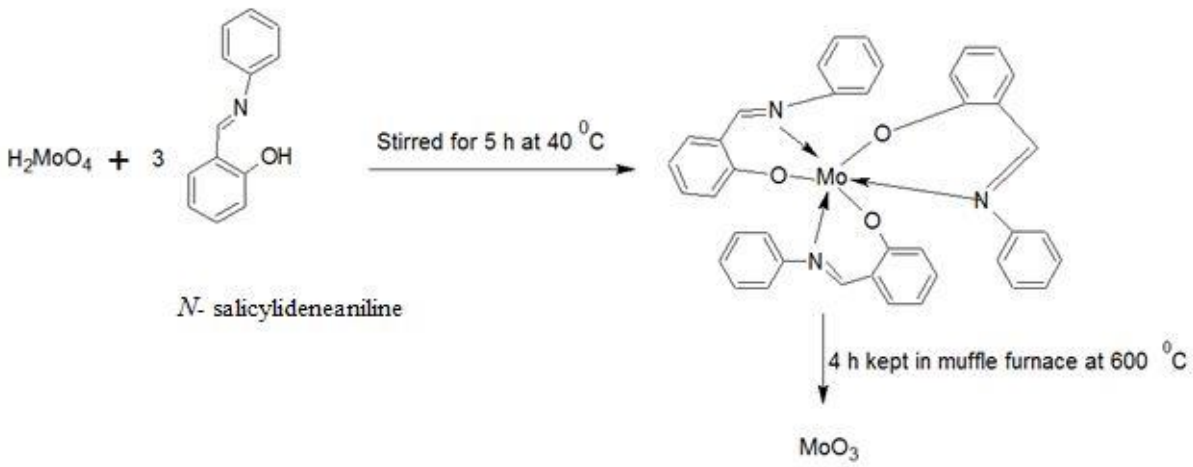

Scheme 2. Synthesis of molybdenum complex with *N*-salicylideneaniline and formation of MoO_3 nanoparticles by complex calcination

4. Characterization of Synthesized Materials

The *N*-salicylideneaniline ($C_{13}H_{11}NO$) ligand was characterised by ^{1}H NMR and ^{13}C NMR using a Bruker EXT 40218 spectrometer. The synthesized molybdenum complex [$Mo(C_{13}H_{10}NO)_3$] and molybdenum trioxide nanoparticles (MoO_3) were analyzed using a Rigaku Smart Lab X-ray diffractometer. TGA-DTA curves were recorded on a Perkin Elmer STA 8000. UV-Visible and FT-IR spectra were obtained using a Shimadzu spectrophotometer (Model MPC-3100) and a Perkin Elmer FT-IR spectrophotometer, respectively. For nano molybdenum trioxide, SEM-EDX analysis was performed with a ZEISS Gemini Instrument and EDX Bucker CAL 4231 and TEM analysis with a FEI-TITAN THEMIS 300 KV.

5. Reagents and Materials

MCF7-human breast adenocarcinoma cell line (From NCCS, Pune), DMEM high glucose cell culture medium (#AT111, Himedia), adjustable multichannel pipettes and a pipettor (Benchtop, USA), foetal Bovine Serum (#RM10432, Himedia), MTT reagent (5 mg/ml) (# 4060 Himedia), dimethyl sulfoxide (#PHR1309, Sigma), Camptothecin (#C9911, Sigma), D-PBS (#TL1006, Himedia), 96-well cell culture plate (Corning, USA), T25 flask (# 12556009, Biolite - Thermo), 50 ml centrifuge tubes (# 546043 TORSON), 1.5 ml centrifuge tubes (TORSON), 10 ml serological pipettes (TORSON), 10 to 1000 µl tips (TORSON). In vitro antibacterial activities were examined for given samples (bulk and NPs). Antibacterial activities of samples against bacteria were investigated by the agar diffusion method. The samples were used for the determination of zones of inhibition or sensitivity against *Escherichia coli*, *Staphylococcus aureus*, *Bacillus* sp. and *Pseudomonas* sp. strains. Antifungal activities of samples against fungi were investigated and samples were used for the determination of zones of inhibition or sensitivity against *Aspergillus* sp. and *Trichoderma* sp.

6. Cell line and Cell Culture of Anticancer Activity Experiment

A 200 µg cell suspension was seeded in a 96-well plate at the required cell density (20,000 cells per well) without the test agent. Cells were allowed to grow for about 24 h at an appropriate concentration and the plate was incubated for 24 h at 37 °C in a 5 % CO_2 atmosphere. The plate was then taken out of the incubator and the spent media was removed. MTT reagent was added to a final concentration of 0.5 mg/mL of the total volume. The plate was wrapped with aluminium foil to avoid exposure to light, and then returned to the incubator for 3 h. (Note: Incubation time varies for different cell lines. Within one experiment, the incubation time should be kept constant for comparison). The MTT reagent was removed and then 100 µg of solubilisation solution (dimethyl sulfoxide) was added. Dissolution was enhanced by gentle stirring in a gyratory shaker. Occasionally, samples were pipetted up and down to completely dissolve the MTT formazan crystals, especially in dense cultures.

7. Cell Viability Assay

The effect of MoO_3 nanoparticles on cell viability was determined using the MTT assay. Briefly, cells (3 x 10^4 cell/mL) were seeded in 96–well plates in 200 µg of a medium containing antibiotics and 10 % FBS. After 24 h the cells were treated with different concentrations of MoO_3. After 48 h 20 µg of MTT solution was added to each well, followed by incubation in a humidified

environment for 4 h. The supernatant was removed and 150 µg of dimethyl sulfoxide was added. The plates were shaken in the dark for 30 min and then analysed with a Sunrise micro plate reader at an absorbance wavelength of 570 nm. Cell viability was recorded as a percentage of the control viability (mean ± SD). The blank contained 200 of RPMI 1640 or DMEM-F12 with 10 % FBS and equivalent reagent concentrations. All experiments were conducted in triplicate [35].

8. Antibacterial Activity Experiment

The antibacterial activities were analysed by the agar diffusion method [36]. The nutrient agar was prepared as per the following composition: peptones 0.5% (concentration), yeast extract 0.3 %, sodium chloride 0.5 %, agar 1.5 %, pH 5.6 ± 0.2, distilled water 1000 mL. The nutrient agar was autoclaved at 121 °C and 15 lbs pressure, then cooled and poured on sterilized petri plates and allowed to solidify. Samples were poured into different plates after solidification and the plates were incubated at 37 °C for 24 h. Bulk molybdenum trioxide was used as a standard for comparison. Antibacterial activity was found to be dependent on the zone of inhibition (in mm). If the inhibition zone was <7 mm, the sample showed less antibacterial activity while if it was >7 mm, then sample showed better antibacterial activity.

9. Antifungal Activity Experiment

The antifungal activities of samples were investigated by employing the agar diffusion method [37]. The samples were used for the determination of their zones of inhibition or sensitivity against *Aspergillus* sp. and *Trichoderma* sp. The antifungal activities were performed on potato dextrose/sabouraud dextrose agar medium. The agar media were prepared as follows: dextrose (glucose) 40 g, peptone 10 g and agar 15 g (pH 5.6 ± 0) were added to 1000 mL distilled water. The solution was autoclaved at 121 °C or 15 lbs pressure and then cooled before being poured into sterilized petri plates and allowed to solidify. A well was made after solidification and the samples were poured into different plates. The plates were incubated at 26-28 °C for 48-72 h, and then observed for zones of inhibition.

RESULTS AND DISCUSSION

1. NMR Spectral Analyses of *N*-salicylideneaniline Ligand ($C_{13}H_{11}NO$)

NMR spectra were recorded of the ligand in dimethyl sulfoxide (d_6) solvent at 25 °C. In the ^{1}H NMR, the presence of nine aromatic protons, one hydroxyl proton (δ 8.94) and one imine proton (δ 13.13) indicated the formation of a new compound. This was further supported by its ^{13}C NMR spectrum, where a signal at δ 163.9 indicated the presence of an imine group in the molecule. Furthermore, a signal at δ 148.5 was due to the carbon of ring (B) attached to a nitrogen. Other aromatic carbon signals appeared at δ 117.1-133.2. Thus the ligand was assigned as N-salicylideneaniline ($C_{13}H_{11}NO$) [38]. ^{1}H NMR (400 MHz, DMSO-d_6): δ_H 6.98-6.99 (d, J = 7.2 Hz, 2H), 7.31-7.39 (d, J = 7.2 Hz, 1H), 7.31-7.46 (m, 5H), 7.65-7.70 (t, J = 7.2 Hz, 1H), 8.94-8.95 (t, J =7.2 Hz, 1H), 13.13 (s, 1H); ^{13}C NMR (100 MHz, DMSO-d_6): δ_C 163.9, 160.0, 148.5, 133.2, 132.0, 129.0, 127.0, 121.0, 119.0, 117.1.

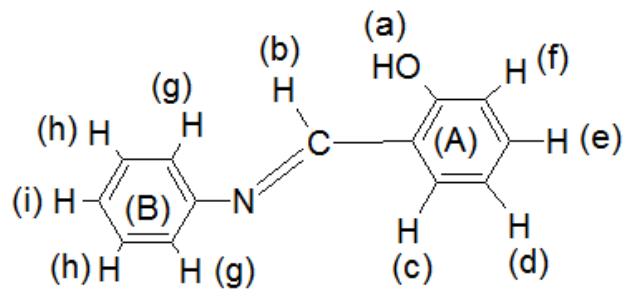

Scheme 3. Structure of *N*- salicylideneaniline (ligand)

2. Preparation and UV-Visible Spectra of Molybdenum Complex/Capping Solution

Molybdic acid (H_2MoO_4) 1.0 g and *N*-salicylideneailine ($C_{13}H_{11}NO$) 2.0 g was added to ethanol (30 mL) and the mixture was stirred at room temperature for 5 h at 40 °C. The solvent was allowed to evaporate and the white colour precipitate obtained was filtered and dried. The absorption spectra of the molybdenum complex [$Mo(C_{13}H_{10}NO)_3$] was determined by UV-visible spectroscopy. The capping solution allows the ligand to stabilize the interface where nanoparticles interact with their medium of preparation. Specific structural features of nanoparticles are attributed to capping on their surface. These stabilizing agents play a key role in altering biological activity. The absorption spectrum of the molybdenum complex displayed two bands at 254 nm and 302 nm, as shown in Figure 1, due to π-π* transitions involving molecular orbitals located on the aromatic moiety in the complex. This clearly shows that metal to ligand charge transfer occurred in the molybdenum complex [39, 40].

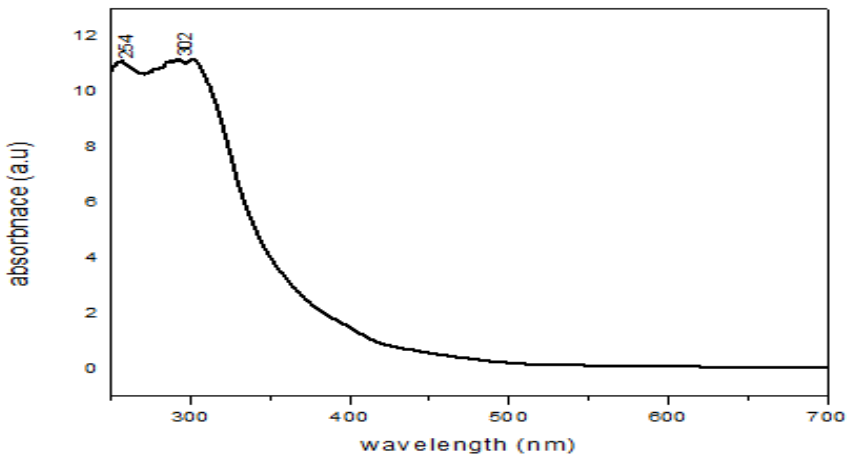

Figure 1. UV-Visible spectra of molybdenum complex with *N*-salicylideneaniline

3. FT-IR Spectrum of Molybdenum Complex with *N*-salicylideneaniline [$Mo(C_{13}H_{10}NO)_3$]

The molybdenum complex with *N*-Salicylideneaniline [$Mo(C_{13}H_{10}NO)_3$] was characterized by its FT–IR spectrum, as shown in Figure 2. The presence of the peak for the molybdenum–nitrogen band at 1070 cm^{-1} was due to the bonding between the central metal ion and the ligand (π-electron delocalization from the metal to the nitrogen atom and resonance interactions with the benzene derivative ring). The absorption band at 910 cm^{-1} and 857 cm^{-1} was attributed to the (Mo–O) stretching mode. The band at around 3193 cm^{-1} was assigned to the stretching vibration of the N–H group. The strong bands at 1609 cm^{-1} indicated the stretching vibration of the -C=N- group, while those at 1589 cm^{-1} and 3666 cm^{-1} O–H were due to the phenolic oxygen moiety in the complex. The peak at 1483 cm^{-1} corresponded to the stretching and bending vibrations of O-H bonds of absorbed water molecules. The molybdenum complex exhibited a strong band at 1722 cm^{-1} due to (C=C). In the IR spectrum of Mo complexes, the band at 1269 cm^{-1} was assigned to (C-O) stretching vibrations. This band was also found in corresponding free ligands such as carbon monoxide (CO) and ammonia (NH_3) at 1177-1136 cm^{-1}. These free ligand peaks are due to the decomposition of molybdenum complexes. The new bands at 544 cm^{-1} and 690 cm^{-1}, and 617 cm^{-1} may be assigned to υ(Mo-O) and υ(Mo-N) stretching. The band at 2927-2860 cm^{-1} may be due to impurities present in the complex [41].

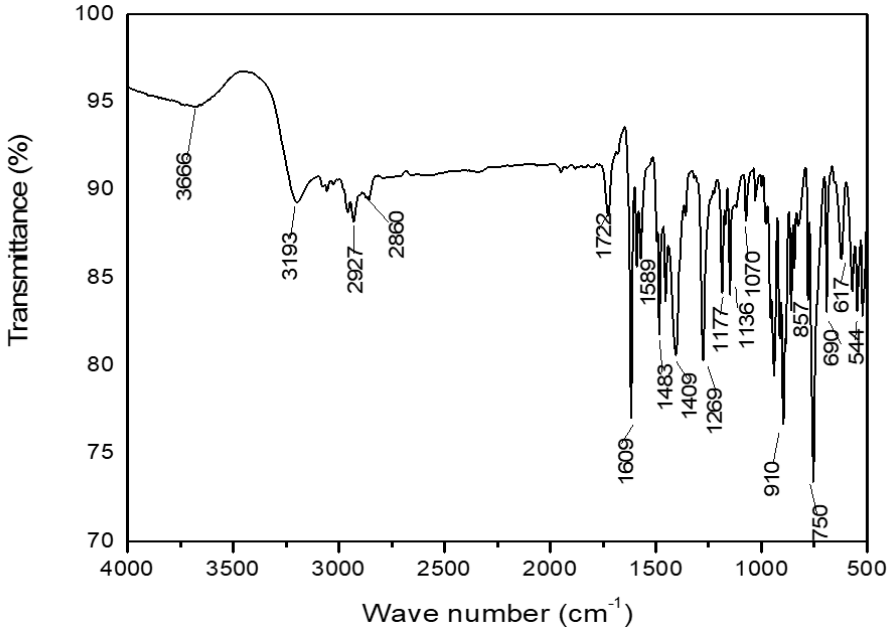

Figure 2. FT-IR spectrum of molybdenum complex with *N*-salicylideneaniline

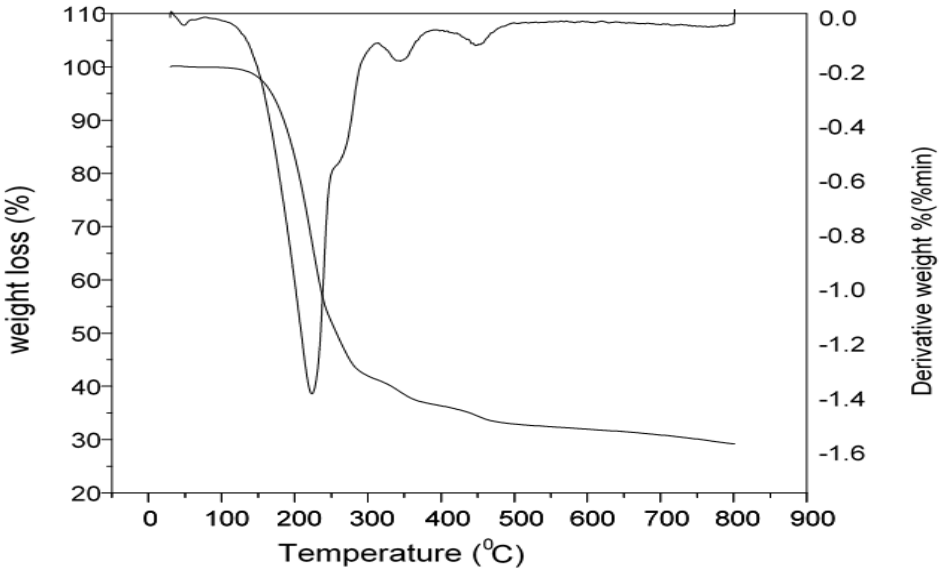

Figure 3. TGA-DTA curves of the molybdenum complex with *N*-salicylideneaniline

4. TGA-DTA Analysis of the Molybdenum of Complex with *N*-salicylideneaniline [$Mo(C_{13}H_{10}NO)_3$]

The thermal stability of the molybdenum complex at 40 °C to 900 °C was studied using a heating rate of 10 °C per minute. The TGA-DTA curves of the molybdenum complex are depicted in Figure 3. The TG curve showed that decomposition occurred at 150 °C. The first stage of decomposition indicated a weight loss of around 40%. Then, thermal decomposition took place between 150 °C and 350 °C. After 350 °C, a mild weight loss was also observed in the sample. On the other hand, the DTA curve showed an endothermic peak at 350 °C, due to decomposition of the molybdenum complex; however, a metal oxide was formed after 350 °C, and this was stable up to 800 °C.

5. Preparation and UV-Visible Spectra of Synthesized Molybdenum Trioxide Nanoparticles (MoO_3)

Molybdenum trioxide nanoparticles (MoO_3) were synthesized from molybdenum N-salicylideneaniline complex [$Mo(C_{13}H_{10}NO)_3$] as precursor. 0.5 g molybdic acid (H_2MoO_4) and 2.0 g N-salicylideneaniline ($C_{13}H_{11}NO$) were added to ethanol (30 mL) and the reaction was allowed to run for 5 h with continuous stirring at 40 ºC. The complex formed was dried at room temperature for 6 days. The complex was ashed in a muffle furnace at 600 °C for 4 h and a white powder was formed. In Figure 4 (A), MoO_3 shows an absorption peak at around 341 nm. The absorption spectrum was further analysed by plotting $(\alpha hv)^2$ against hv or energy based on Equation 1,

$$(\alpha hv)^2 = A(hv-Eg)^n \ldots\ldots\ldots\ldots\ldots\ldots (1)$$

where α is the absorption coefficient, A is a constant independent of frequency v, n is the exponent that depends upon the quantum selection rules for the particular material and Eg is the band gap of the material. This relationship gives Eg by extrapolating the straight portion of $(\alpha hv)^2$ against hv in the plot shown in Figure 4 (B). Synthesized MoO_3 nanoparticles show a band gap energy of approximately 2.8 eV [42]. This result is in agreement with other studies reporting a band gap for orthorhombic phase of MoO_3 of approximately have great absorption at both ultraviolet and visible regions [43-47].

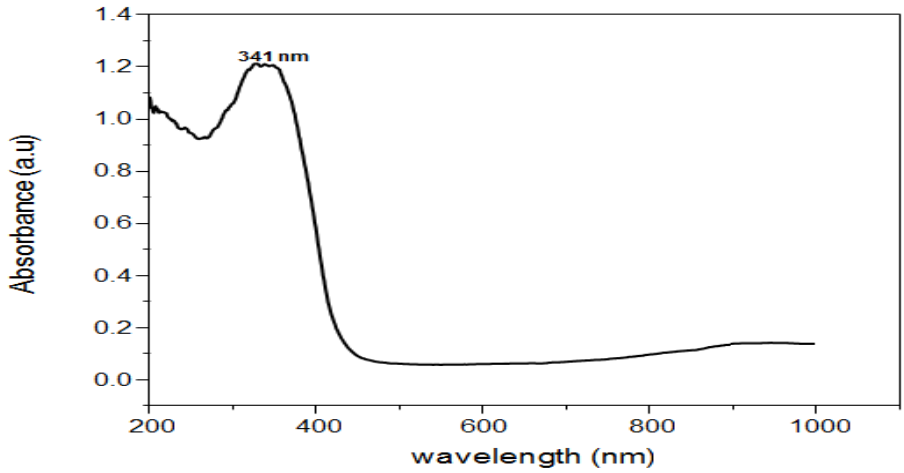

Figure 4 (A). UV-visible absorption spectrum of molybdenum trioxide nanoparticles (MoO_3)

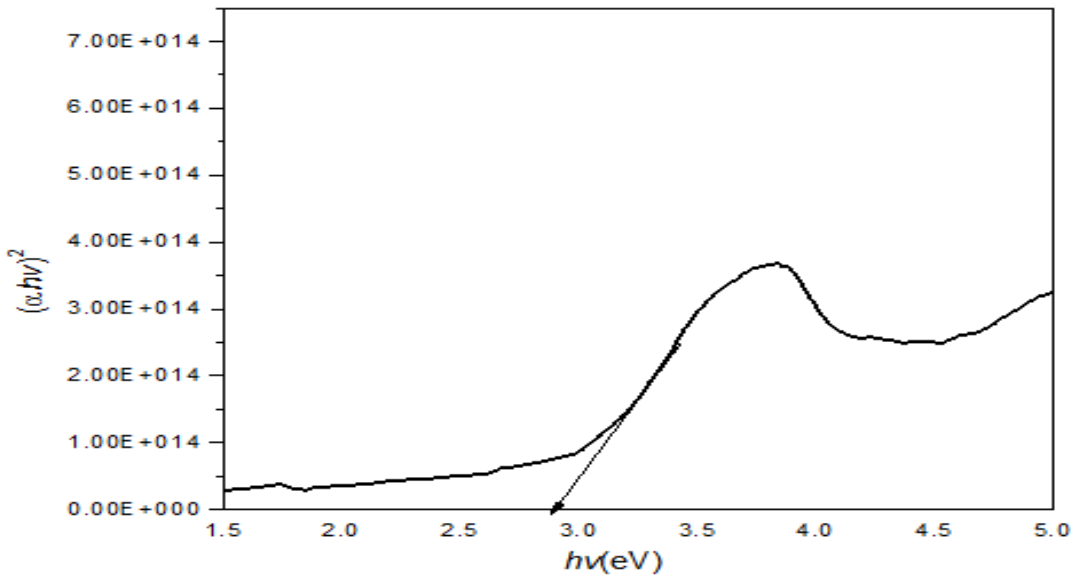

Figure 4 (B). UV-visible absorption band gap spectrum of molybdenum trioxide nanoparticles (MoO_3)

6. FT-IR of Molybdenum Trioxide Nanoparticles (MoO_3)

The composition and quality of the material was investigated by FT-IR spectroscopy. The FT-IR spectrum of the orthorhombic phase of MoO_3 nanoparticles is shown in Figure 5. The spectrum shows three strong peaks: 993 cm^{-1}, attributed to the terminal M=O stretching vibration, with an indicator of the layered orthorhombic MoO_3 phase, 866 cm^{-1} to the stretching mode of oxygen in Mo–O–Mo bonds, and a broad band at 572 cm^{-1} to the bending vibration of oxygen and Mo. A peak at 1723 cm^{-1} was associated with the vibration mode of the O–H bond of adsorbed water molecules [48-50].

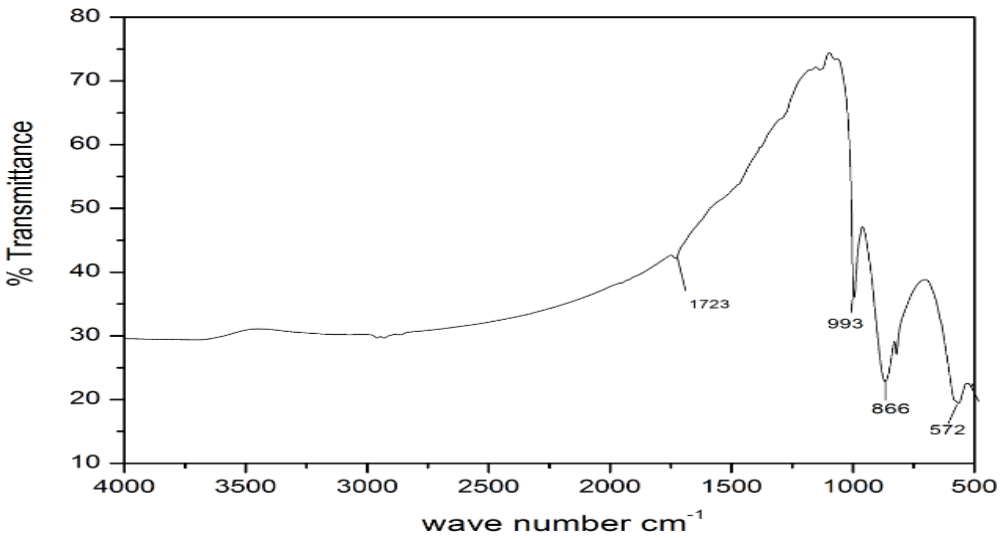

Figure 5. FT-IR spectra of molybdenum trioxide nanoparticles (MoO_3)

7. PXRD Analysis of Molybdenum Trioxide Nanoparticles (MoO_3)

Figure 6 represents the powder XRD pattern of MoO_3. The wavelength used for PXRD analysis was Cu Kα-1.540 (Å). It was found that the peaks corresponding to (020), (110), (040), (021), and (200) were of the orthorhombic crystal structure of MoO_3. This was found to be highly crystalline in nature using the Debye Scherrer Equation: $D=k\lambda/d \cos\theta$, where d is the full width at half maximum or half-width in radians, k is the crystallite shape factor, which usually takes a value of about 0.9 and λ the wavelength of the X-ray source used in PXRD, found to be 30-47 nm from peak broadening. The average crystallite size (D) of prepared MoO_3 nanoparticles was calculated and found to be 35 nm. This value is consistent with the TEM observations [51-55].

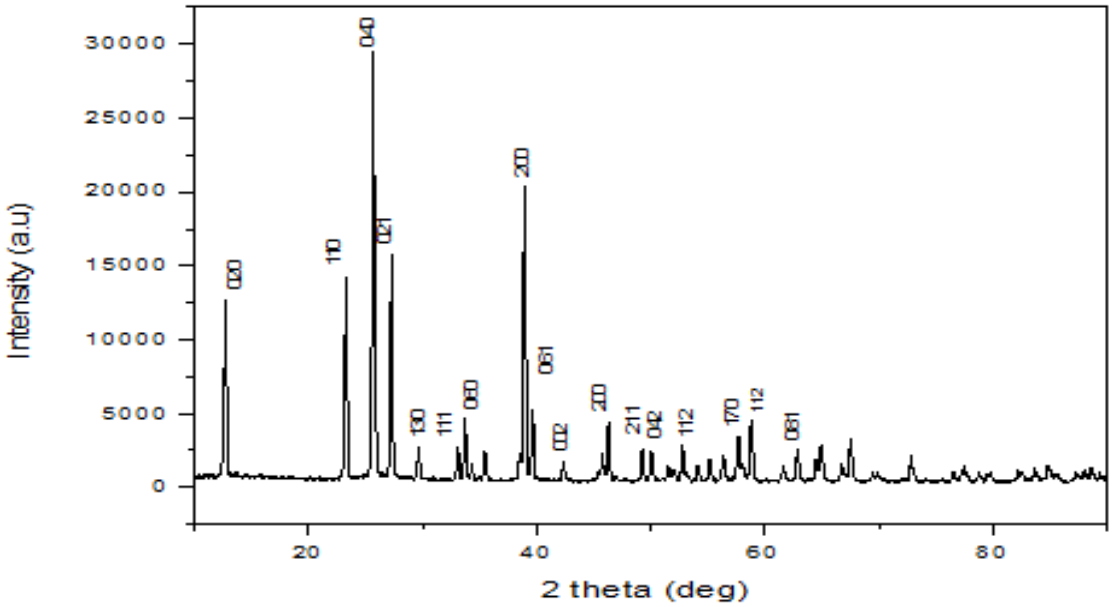

Figure 6. PXRD pattern of molybdenum trioxide nanoparticles (MoO_3)

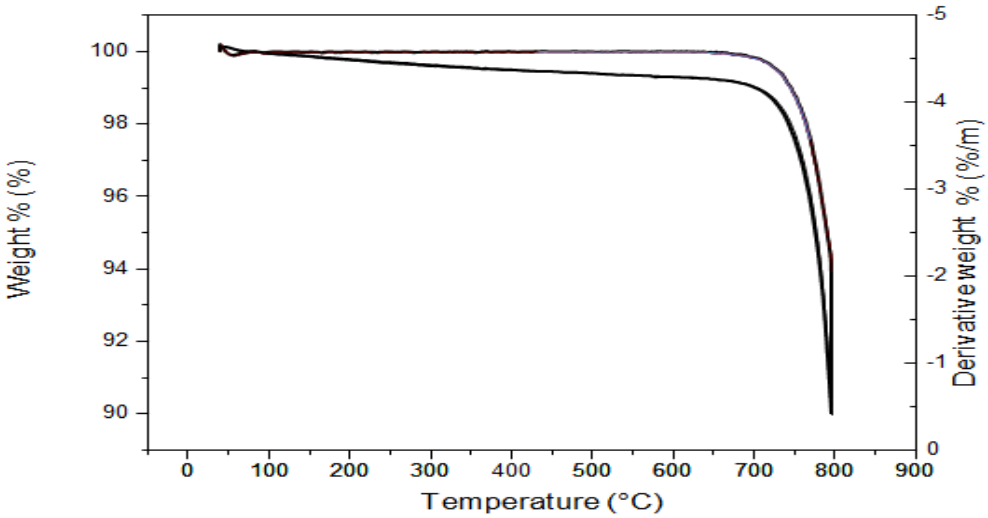

Figure 7. TGA-DTA curves of molybdenum trioxide nanoparticles (MoO_3)

8. TGA-DTA Analysis of Molybdenum Trioxide Nanoparticles (MoO_3)

Thermogravimetric analysis (TGA) and differential thermal analysis (DTA) play an important role in understanding the thermal stability and relative weight loss of the material [56]. The analysis was performed under a nitrogen atmosphere of 20 cm^3 m^{-1} at a temperature range from 40 °C to 900 °C, at 10 °C per min. The thermal graph is shown in the Figure 7. It is noted that molybdenum trioxide nanoparticles were stable up to 800 °C as there was negligible weight loss. The slight weight loss in the sample resulted mainly due to evaporation of water molecules from voids in the synthesized nanopowder.

9. SEM and EDX of Molybdenum Trioxide Nanoparticles (MoO_3)

An SEM image of the MoO_3 orthorhombic crystal structure is shown in Figure 8. The micrograph exhibits the formation of nanoparticles of MoO_3. It is fairly clear that most of the particles are approximately spherical in shape and the particle size ranged from 30-47 nm. From the images, it can be confirmed that the particles are smaller in size [57]. To check the chemical composition of the material, an EDX spectroscopy analysis was performed. The EDX spectra of MoO_3 nanoparticles showed that the surface of MoO_3 comprised Mo and O (Figure 9).

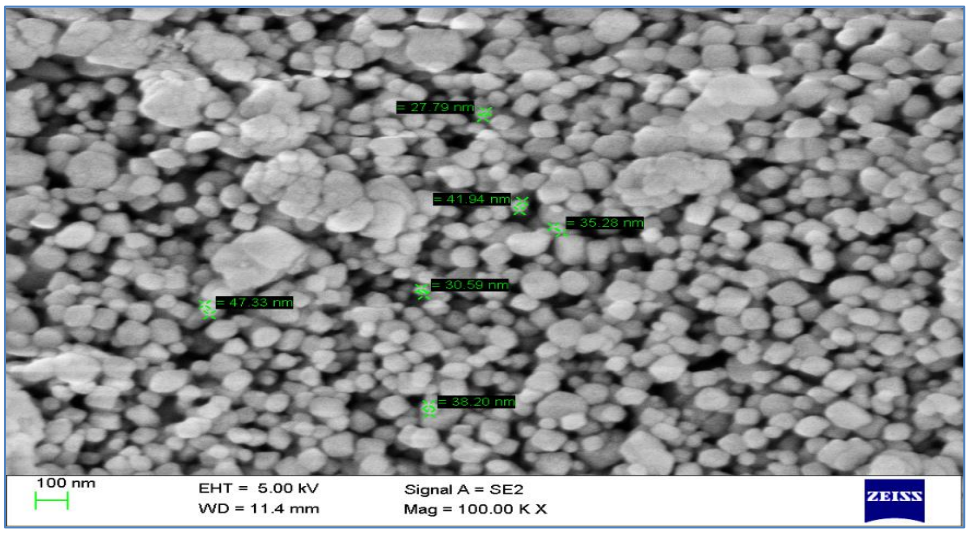

Figure 8. SEM image of molybdenum trioxide nanoparticles (MoO_3)

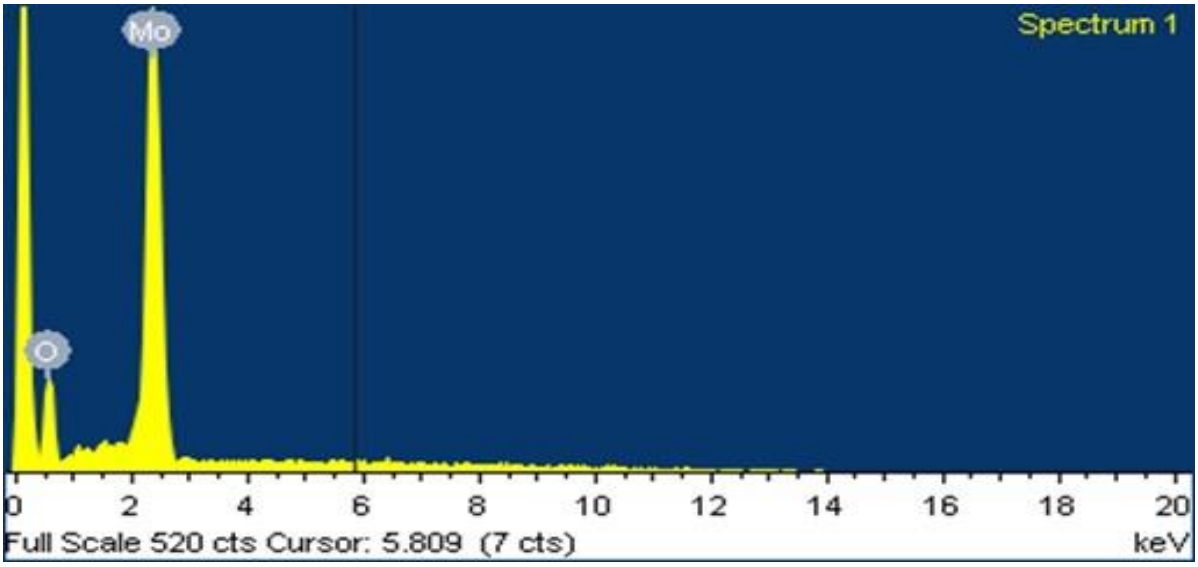

Figure 9. EDX spectrum of molybdenum trioxide nanoparticles (MoO_3)

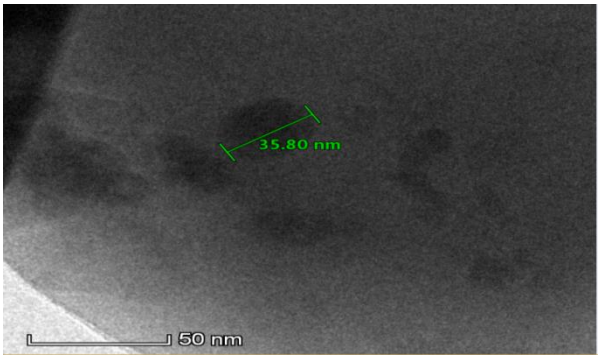

Figure 10. TEM image of MoO_3 nanoparticles

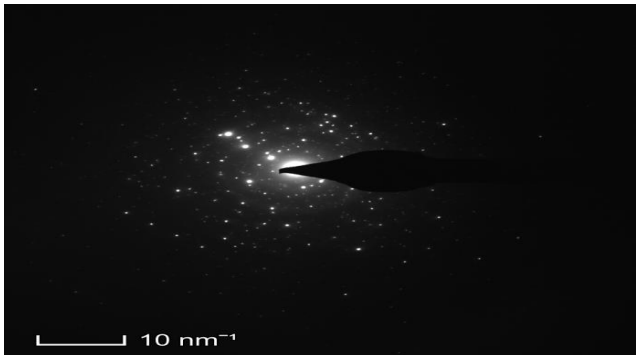

Figure 11. TEM CBED pattern of MoO_3 nanoparticles

10. TEM Image of Molybdenum Trioxide Nanoparticles (MoO_3)

A TEM microscopic study was done to determine the surface morphology of synthesized MoO_3. The TEM microstructure in Figure 10 clearly indicates the formation of nanoparticles in the 35 nm size range. Convergent beam electron diffraction (CBED) pattern provided information about the crystallinity of the prepared sample. MoO_3 was found to be perfectly spherical in nature (Figure 11).

11. Anticancer Activity

The cytotoxicity profile of MoO_3 was examined against the bulk MoO_3 human breast cancer cell line MCF7 using an MTT assay. In this study, two tested compounds were evaluated to check their cytotoxicity activity towards MCF-7. The concentrations of the compounds used to treat the cells are given in Table 1 [58-60].

The statistical data from the MTT cytotoxicity study suggest that bulk MoO_3 and MoO_3 NPs showed potential cytotoxic properties against MCF7 cells, with IC_{50} concentrations of 190.23 μg/mL and 78.64 μg/mL compared to the standard drug, Camptothecin for which 10 μg/mL was used in this study. The results suggest that the MoO_3 NPs may have significant anticancer potential against human breast cancer cells due to their low IC_{50} value.

Table 1. Drug treatment at different concentrations

Sl. No	Test Compounds	Cell Line	Concentration
1	Untreated	MCF7	-
2	Standard (Camptothecin)	MCF7	10 µg/mL
3	Blank	-	-
4	Bulk MoO_3	MCF7	12.5,25,50,100,200 µg/mL
5	Nanoparticles of MoO_3 (NPs)	MCF7	12.5,25,50,100,200 µg/mL

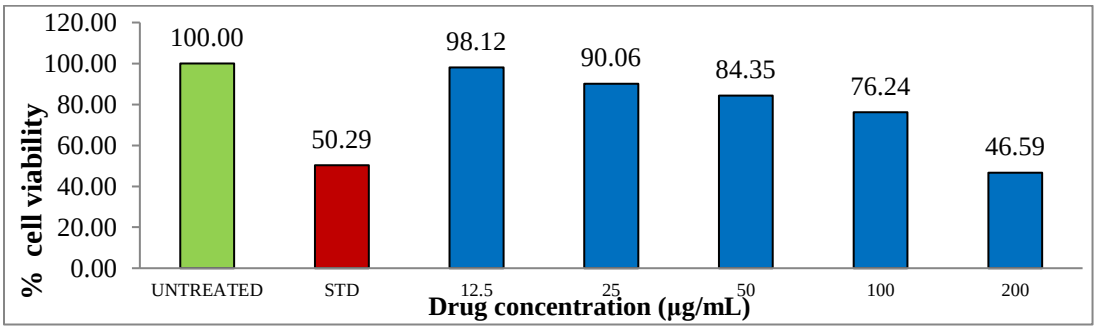

Figure 12. Cell viability of MCF7 cells treated with bulk MoO_3 at different concentrations in comparison to the control

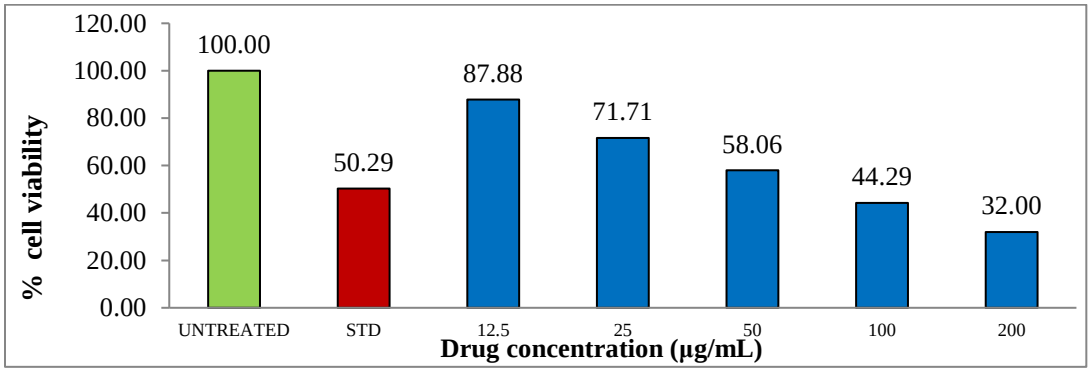

Figure 13. The cell viability (%) of MCF7 cells treated with MoO_3 NPs at different concentrations in comparison to the control

Table 2. IC_{50} concentration of bulk MoO_3 and MoO_3 NPs against MCF7 cells

Sl .No	Sample Code	IC_{50} (µg/mL)
1	Bulk MoO_3	190.23
2	MoO_3 NPs	78.64

12. Antibacterial Activity

According to previous studies, the metal oxides carry positive charges while microorganisms carry negative charges; this causes an electromagnetic attraction between the microorganism and the metal oxide which leads to oxidization, causing pits or holes in the bacterial cell wall. This could be associated with internalized particles, leading to increased permeability and cell death [61]. Molybdenum trioxide nanoparticles, due to their small size and high surface to volume ratio, undergo a higher level of interaction with the bacterial cell surface than large particles, resulting in good antibacterial activity [62,63]. The antibacterial activity assay of molybdenum trioxide nanoparticles was carried out using the agar diffusion method against two Gram-positive bacteria i.e. *S. aureus*, *Bacillus* sp. and two Gram-negative bacteria, *Pseudomonas* sp. and *E. coli*, for two different concentrations as shown in Figure 14 for the bulk sample and Figure 15 for the nanoparticle sample of molybdenum trioxide. 50µl/mL and 100 µl/mL concentrations of bulk molybdenum trioxide were used as standards at the same concentration.

Table 3. In vitro antibacterial screening of synthesized bulk molybdenum trioxide

Sample	Concentration in µL	*S. aureus*	*E. coli*	*Bacillus* sp.	*Pseudomonas* sp.
		Diameter of zone of inhibition in mm			
bulk	25 µg/mL (50 µL/mL)	3	4	2	3
	25 µg/mL (100 µL/mL)	3	3	2	1

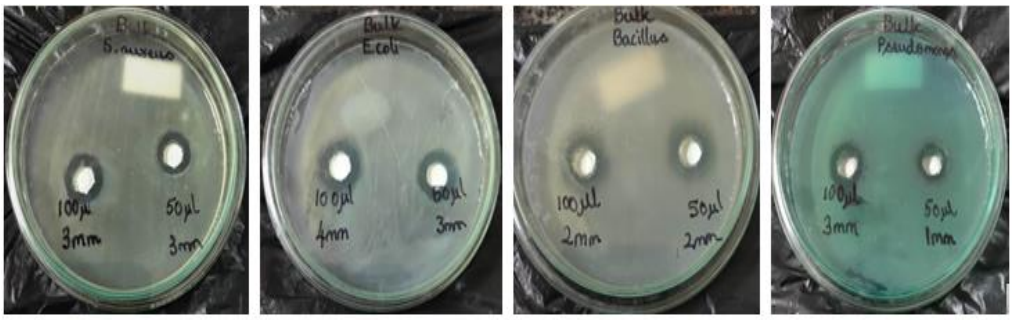

bulk-*S.aureus* bulk-*E. coli* bulk-*Bacillus* sp bulk-*Pseudomonas* sp

Figure 14. Antibacterial activity of the bulk sample

Table 4. In vitro antibacterial screening of synthesized molybdenum trioxide NPs

Sample	Concentration in µL	*S. aureus*	*E. coli*	*Bacillus* sp.	*Pseudomonas* sp.
		Diameter of zone of inhibition in mm			
NPs	25 µg/mL (50 µL/mL)	0.5	0.5	0.5	0.5
	25 µg/mL (100 µL/mL)	0.5	0.5	0.5	1
	25 µg/mL (200 µL/mL)	3	4	3	2
	25 µg/mL (300 µL/mL)	5	5	10	10

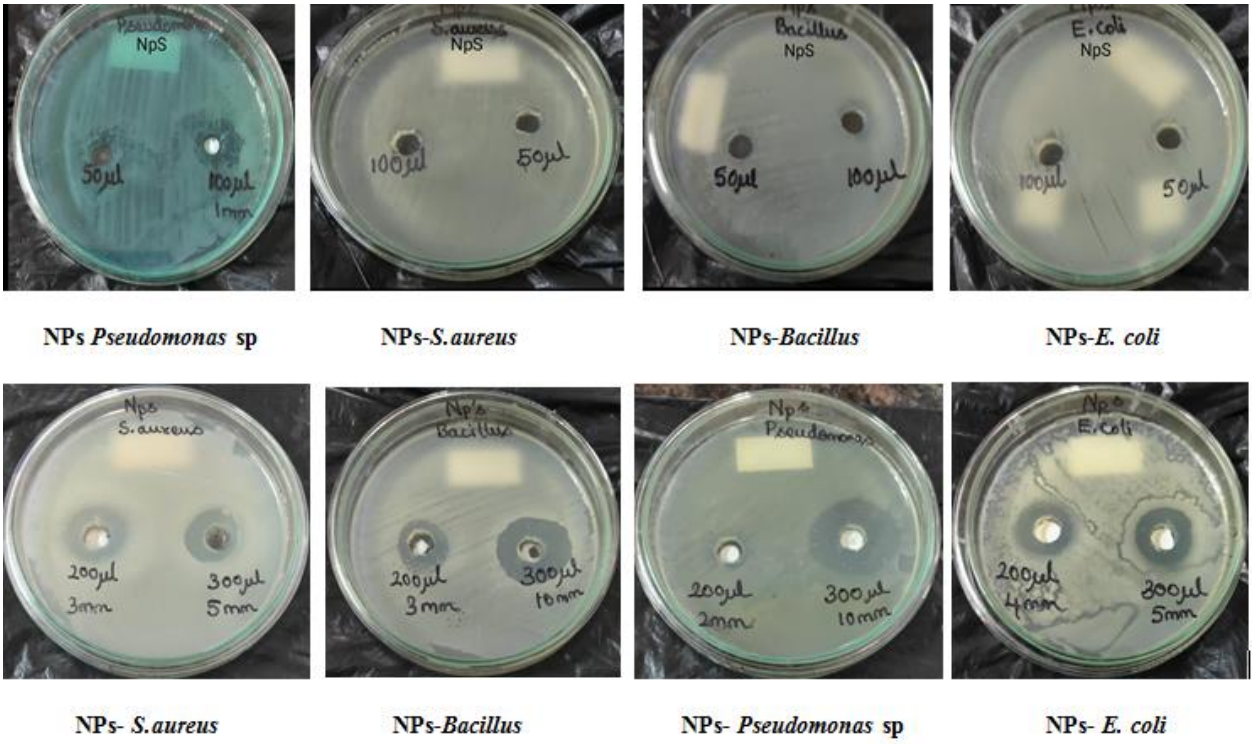

Figure 15. Antibacterial activity of NP sample

13. Antifungal Activity

The antifungal activity of bulk and NPs samples were recorded against *Aspergillus* sp. and *Trichoderma* sp. in 50 µL concentrations, which did not show any activity against both fungal cultures. In the case of the molybdenum trioxide nanoparticles, 100 µL showed 3 mm and 2 mm zones of inhibition against *Aspergillus* sp. and *Trichoderma* sp. respectively, as shown in Table 5. Thus the nanoparticle sample had a higher potential to kill fungi than the bulk sample. The bulk sample at 100 µL did not show any activity against both cultures. NPs at concentrations of 200 µL and 300 µL showed 2 mm and 5 mm zones of inhibition against *Aspergillus* sp. respectively, and 1 mm and 4 mm against *Trichoderma* sp. respectively. This suggested that the bulk sample had less potential activity than the nanoparticles.

Table 5. Antifungal activity of bulk and NPs molybdenum trioxide at different concentrations

Sample	**Concentration in µL**	***Aspergillus* sp.**	***Trichoderma* sp.**
	Diameter of Zone of inhibition in mm		
bulk	25 µg/mL (50 µL/mL)	-	-
	25 µg/mL (100 µL/mL)	3	2
NPs	25 µg/mL (50 µL/mL)	-	-
	25 µg/mL (100 µL/mL)	-	-
	25 µg/mL (200 µL/mL)	2	1
	25 µg/mL (300 µL/mL)	5	4

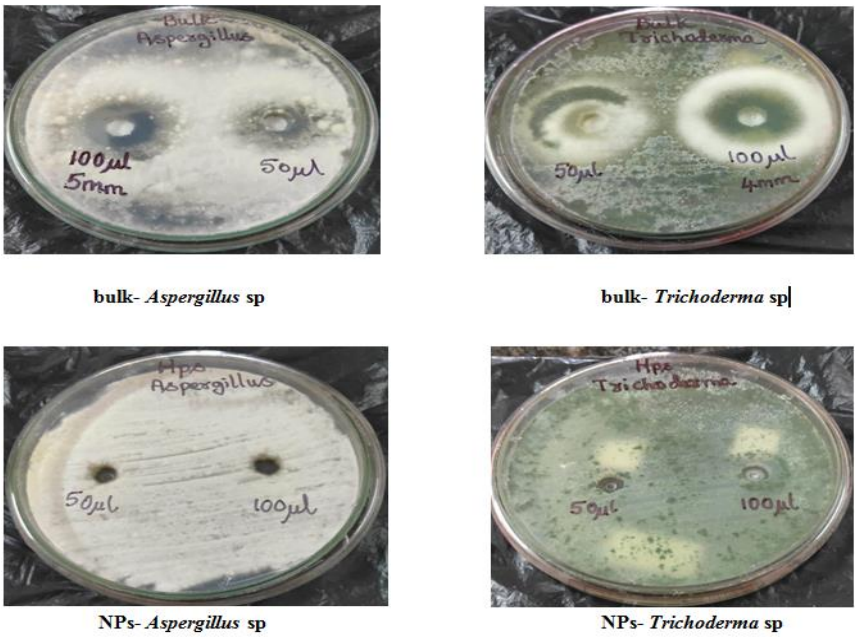

bulk- ***Aspergillus*** **sp**

bulk- ***Trichoderma*** **sp**

NPs- ***Aspergillus*** **sp**

NPs- ***Trichoderma*** **sp**

Figure 16. Antifungal activity of bulk and NP samples

CONCLUSION

In the current study, molybdenum trioxide nanoparticles (MoO_3) were successfully synthesized from a molybdenum complex of salts using *N*-salicylideneaniline [$Mo(C_{13}H_{10}NO)_3$] ligands. The ligand played a significant role in controlling particle size**.** The SEM microstructure clearly indicated the formation of spherical nanoparticles in the range of 30-47 nm. TGA analysis revealed the stability of the synthesized compound at high temperatures**.** In terms of anticancer activity of the given test compounds, bulk MoO_3 and MoO_3 NPs showed IC_{50} concentrations of 190.23 µg/mL and 78.64 µg/mL, respectively, against the MCF7 cells after 24 h of incubation at 37 °C. The observations strongly suggest that the MoO_3 NPs may have possible therapeutic potential against human breast cancer cells based on the dosage of the drug after an incubation period of 24 h. The obtained values for the zone of inhibition for Gram-positive and Gram-negative strains suggest that the prepared MoO_3 NPs showed excellent antibacterial activity and can be used as promising antibacterial agents. The effect was dose dependent, and more pronounced against Gram-positive organisms than Gram-negative ones. The results of the antimicrobial screening were statistically significant. The antifungal activity of bulk and NP samples were tested against *Aspergillus* sp. and *Trichoderma* sp. In 50 µL/mL concentrations, both bulk MoO_3 and MoO_3 NPs did not show any activity against both fungal cultures. For the bulk sample, 100 µL/mL showed 3 mm and 2 mm zones of inhibition against *Aspergillus* sp. and *Trichoderma* sp. The NP sample at 100 µL/mL showed no activity against both cultures. At 200 µL/mL and 300 µL/mL it showed 2 mm and 5 mm zones of inhibition against *Aspergillus* sp. respectively, and 1 mm and 4 mm against *Trichoderma* sp. respectively. From these results, we are confident that our MoO_3 NPs are a very efficient biologically-active material against cancer, bacteria, and fungi.

ACKNOWLEDGEMENT

Sincere thanks to the Principal, Dr. Sr. Lalitha Thomas and Management of Jyoti Nivas College Autonomous, and the Chemistry Department of Bangalore University for extending their support and providing the infrastructure to carry out the research work. We are thankful to the Sophisticated Instrumentation Facility (SIF), School of Advanced Sciences Chemistry Division, Vellore Institute of Technology (VIT), Vellore, the Department of Inorganic and Physical Chemistry, Centre for Nano Science and Engineering (CENSE), Indian Institute of Science (IISc) and the Scientific and Industrial Research Center Bangalore.

REFERENCES

1. Botteon, C. E. A., Silva, L. B., Ccana-Ccapatinta, G. V., Silva, T. S., Ambrosio, S. R., Veneziani, R. C. S., Bastos, J. K. and Marcato, P. D. (2021) Biosynthesis and characterization of gold nanoparticles using brazilian red propolis and evaluation of its antimicrobial and anticancer activities. *Nature Research*, **11**.

2. Gula, A. R., Shaheenb, F., Rafiquea, R., Bala, J., Waseemb, S. and Park, T. J. (2020) Grass-mediated

biogenic synthesis of silver nanoparticles and their drug delivery evaluation: a biocompatible anti-cancer therapy. *Chemical Engineering Journal,* **407**, 127−202.

3. Burke, A. R., Singh, R. N., Carroll, D. L., Wood, J. C., D'Agostino, R. B. Jr., Ajayan, P. M., Torti, F. M. and Torti, S. V.(2012) P-glycoprotein-targeted photothermal therapy of drug-resistant cancer cells using antibody-conjugated carbon nanotubes biomaterials, **33**, 2961−2970.

4. Sanpui, P., Chattopadhyay, A. and Ghosh, S. S. (2011) Induction of apoptosis in cancer cells at low silver nanoparticle concentrations using chitosan nanocarrier. *ACS Appl. Mater. Interfaces*, **3**, 218−228.

5. Premanathan, M., Karthikeyan, K., Jeyasubramanian, K. and Manivannan, G. (2011) Selective toxicity of ZnO nanoparticles toward Gram-positive bacteria and cancer cells by apoptosis through lipid peroxidation nanomedicine: *NBM*, **7**, 184−192.

6. Raghupathi, K. R., Koodali, R. T. and Manna, A. C. (2011) Size-dependent bacterial growth inhibition and mechanism of antibacterial activity of zinc oxide nanoparticles. *Langmuir*, **5,** 4020−4028.

7. Calixto, G. M. F., Jéssica Bernegossi, J., Freitas, L. M. D., Carla Raquel Fontana, C. R. and Marlus Chorilli, M. (2016) Nanotechnology-based drug delivery systems for photodynamic therapy of cancer. *A Review Molecules*, **3**, 21.

8. Hu, Z., Li, J., Li, C., Zhao, S., Li, N., Wang, Y., Wei, F., Chen, L. and Huang, Y. (2013) Folic acid-conjugated graphene–ZnO nano hybrid for targeting photodynamic therapy under visible light irradiation. *J. Mater. Chem. B*, **1**, 5003−5013.

9. Shen, J. M., Yin, T., Tian, X.-Z., Gao, F.-Y. and Xu, S. (2013) Surface charge-switchable polymeric magnetic nanoparticles for the controlled release of anticancer drug. *ACS Appl. Mater. Interfaces*, **5**, 7014−7024.

10. Tran, T. A., Krishnamoorthy, K., Song, Y. W., Cho, S. K. and Kim, S. J. (2014) Toxicity of nano molybdenum trioxide toward invasive breast cancer cells. *Appl. Mater. Interfaces,* **6(4)**, 2980–2986.

11. Harada, A., Ono, M., Yuba, E. and Kono, K. (2013) Titanium dioxide nanoparticle-entrapped polyion complex micelles generate singlet oxygen in the cells by ultrasound irradiation for sonodynamic therapy. *Biomater. Sci.*, **1**, 65−73.

12. Yang, K., Wan, J., Zhang, S., Tian, B., Zhang, Y. and Liu, Z.(2012) The influence of surface chemistry and size of nanoscale graphene oxide on photothermal therapy of cancer using ultra-low laser power. *Biomaterials*, **33**, 2206−2214.

13. Romeroa, N. Z., Migue, A., Camacho-Lopezb, C., Nestorc, A. R.V., Castrejon-Sanchezd, V. H., Aguilare , G., Camacho-Lopezf, S. and Camacho-Lopezg, M. (2019) Synthes is of molybdenum oxide nanoparticles by nanosecond laser ablation Materials. *Chemistry and Physics*, **240**, 122163.

14. Nitin Dighore, N., Jadhav, S., Anandgaonker, P., Gaikwad, S. and Rajbhoj, A. (2016) Molybdenum oxide nanoparticles as antimicrobial agents. *J Clust Sci.*

15. Fakhri, A. and Nejad, P. A. (2016) Antimicrobial, antioxidant and cytotoxic effect of molybdenum trioxide nanoparticles and application of this for degradation of ketamine under different light illumination. *J. of Photochemistry & Photobiology, B: Biology*, **159**, 211–217.

16. Matin, M. M., Chakraborty, P., Alam, M. S., Islam, M. M. and Hanee, U. (2020) Novel mammopyranoside esters as sterol 14α-demethylase inhibotors: Synthesis, PASS prediction, moleculardocking, and pharmacokinetic studies. *Carbohydr. Res.*, **496**, 108130. https://doi.org/10.1016/j.carres.2020.108130.

17. Bao, T. (2016) Preparation of molybdenum oxide nanomaterials and their applications in tumor diagnosis and treatment [D]. CNKI:CDMD:2. 1016.227226.

18. Neuberger, T., Schopf, B., Hofmann, H., Hofmann, M. and Von Rechenberg, B. (2005) Superparamagnetic nanoparticles for biomedical applications: possibilities and limitations of a new drug delivery system. *J. Magn Mater.*, **293,** 483–496.

19. Bonilla, J. J. A., Guerrero, D. J. P., Clara I., Sa´nchez Suarez, C. I. S., López, C. C. O. and Sáez, R. G. T. (2015) In vitro antifungal activity of silver nanoparticles against fluconazole-resistant candida species. *World J. Microbiol. Biotechnol.*, **31**, 1801–1809.

20. Owaid, M. N., Raman, J., Lakshmanan, H., Al-Saeedi, S. S.S., Sabaratnam, V. and Ali Abed, I. (2015) Mycosynthesis of silver nanoparticles by pleurotus cornucopiae var. citrinopileatus and its inhibitory effects against candida sp. *Mater. Lett.*, **153,** 186–190.

21. Castro, R. D., de Souza, T. M. P. A., Bezerra, L. M. D., Ferreira, G. L. S., de Brito Costa, E.M. M. and Cavalcanti, A. L. (2015) Antifungal activity and mode of action of thymol and its synergism with nystatin against candida species involved with infections in the oral cavity: an in vitro study. *BMC Complement. Altern. Med.*, **15,** 1–7.

22. Thevenot, P., Cho, J., Wavhal, D., Timmons, R. B. and Tang, L.(2008) Surface chemistry influences cancer killing effect of TiO_2 nanoparticles. *Nanomedicine,* **4**, 226−236.

23. Lin, W., Huang, Y. W., Zhou, X. D. and Ma, Y. (2006) In vitro toxicity of silica nanoparticles in human lung cancer cells. *Int. J. Toxicol.*, **25**, 451−457.

24. Vinarde, M. P. and Mitjans, M. (2015) Antitumor activities of metal oxide nanoparticles. *Nanomaterials,* **5**, 1004−1021.

25. Krishnamoorthy, K., Moon, J. Y., Hyun, H. B., Cho, S. K. and Kim, S. -J. (2012) Mechanistic investigation on the toxicity of MgO nanoparticles toward cancer cells. *J. Mater. Chem.*, **22**, 24610−24617.

26. Christiansen, T. L., Bojesen,D., Juelsholt, M., Etheridge, J. and Jensen, K. M. O. (2019) Size induced structural changes in molybdenum oxide nanoparticles. *ACS Nano.*, **13(8)**, 8725–8735.

27. Dahal, N. N., Garcia, S., Zhou, J. and Humphrey, S. M. (2012) Beneficial effects of microwave-assisted heating versus conventional heating in noble metal nanoparticle synthesis. *ACS Nano.*, **6**, 9433−9446.

28. Soltani, M. T., Djouama, A., Boutarefala, A. and Poulain, M. (2009) New heavy metal oxide glasses based on Sb_2 O_3.. *J. Optoelectron. Adv. Mater.*, **1**, 339−342.

29. Afsharpour, M., Mahjoub, A. and Amini, M. M.(2009) Synthesis of molybdenum oxide nanohybrids as efficient catalysts in oxidation of alcohols. *Journal of Inorganic and Organometallic Polymers and Materials,* **19(3)**, 298−305.

30. Shukoor, M. I., Therese, H. A, Gorgishvili, L., Glasser, G., Kolb, U. and Tremel, W. (2006) From layered molybdic acid to lower-dimensional nanostructures by intercalation of amines under ambient conditions. *Chem. Mater.*, **18**, 2144.

31. Bilecka, I., Djerdj, I. and Niederberger, M. (2008) One-minute synthesis of crystalline binary and ternary metal oxide nanoparticles. *Chem. Commun.*, **13**, 886−888.

32. Lee, Y. J., Yi, J., Gao, G. F., Koerner, H., Park, K., Wang, J., Luo, K., Vaia, R. A. and Hsu, J. W. P. (2012) Low-temperature solution-processed molybdenum oxide nanoparticle hole transport layers for organic photovoltaic devices. *Adv. Energy Mater.*, **2**, 1193-1197.

33. Anbarasu, S. and Devarajan, P. A. (2014) A phase matchable nonlinear optical crystal salicylideneaniline: Synthesis, growth and characterization. *Optik,* **1**, 125, 333−337.

34. Viswanath, A. V., A. K., Gopinath, C. S. and Vijayamohanan, K. J. (2006) Production of molybdneum trioxide nanosheets by liquid exfoliation and their application and their application in high-performnace supercapacitors. *Appl. Phy.*, **100**, 074319.

35. MTT Cell Proliferation Assay Instruction Guide – ATCC, VA, USA www.atcc.org.

36. Muhammad, D., Matin, M. M., Miah, S. M. R. and Devi, P. (2021) Synthesis, antimicrobial and DFT studies of some benzyl 4-O-acyl-α-L-rhamnopyra-nosides. Orbital. *Electronic J. Chem.*, **13(3)**, 250-258. http://dx.doi.org/10.17807/orbital. vl3i3.1614.

37. Matin, M. M., Uzzaman, M., Chowdhury S. A. and. Bhuiyan, M. M. H. (2021) In vitro antimicrobial, physicochemical, pharmacokinetics , andmolecular docking studies of benzoyl uridine estersagaint SARS-CoV-2 main protease. *Journal of Biomolecular Sturcture and Dynamics,* https://doi.org/10.1080/07391102.1850358; PMID: 33297848;PMCID: PMC7738211.

38. Kumara, N., George, B. P. A., Abrahamse, H., Parashar, V. and Ngila, J. C. (2016) Sustainable one-step synthesis of hierarchical microspheres of PE gylated MoS_2 nanosheets and MoO_3 nanorods: their cytotoxicity towards lung and breast cancer cells. *Applied Surface Science,* **396**.

39. Nazıra, H., Yıldızb, M. M., Yılmaz, H., Tahir, M. N. and Ulku, D. (2000) Intramolecular hydrogen bonding and tautomerism in schiff bases. structure of N-(2-pyridil)-2-oxo-1-naphthylidenemethyla-mine. *Journal of Molecular Structure,* **524**, 241–250.

40. Khalil, M. and Al-Seif, F. A. (2008) Molybdenum and tungsten tricarbonyl complexes of isatin with triphenylphosphine. *Research Letters in Inorganic Chemistry,* **4**.

41. Bagherzadeh, M., Amini M., Ellern, A. and Woo, L. K.(2011) Catalytic efficiency of a novel complex of

oxoperoxo molybdenum(VI): synthesis, x-ray structure and alkane oxidation, *Inorganic Chemistry Communications*, **15**, 52−55.

42. Saheb,V., Sheikhshoaie I. and Stoeckli-Evans, H. A. (2012) Novel tridentate schiff base dioxo-molybdenum(VI) complex: synthesis, experimental and theoretical studies on its crystal structure, ftir, uv–visible, 1 H NMR and 13C NMR spectra spectrochimica acta part a: *Molecular and Biomolecular Spectroscopy*, **95**, 29−36.

43. Sreedhara, M. B., Ramakrishna Matte, H. S. S., Govindaraj, A. and Rao, C. N. R. (2013) Synthesis, characterization, and properties of few-layer MoO_3 chemistry, *Asian journal*, **8**.

44. Duque, J. S., Madrigal, B. M., Riascos, H. and Avila, Y. P. (2019) Colloidal metal oxide nanoparticles prepared by laser ablation technique and their antibacterial test. *Colloids.Interfaces*, **3**, 25.

45. Manifacier, J. C., Murcia, M. D., Fillard, J. P. and Vicario, E. (1997) Optical and electrical properties of SnO_2 thin films in relation to their stoichiometric deviation and their crystalline structure thin Solid Films. *Material Science*, **41**, 127–135.

46. Chithambararaj, A. and Bose, A. A. C. (2011) Hydrothermal synthesis of hexagonal and orthorhombic MoO_3 nanoparticles. *Journal of Alloy and Compounds*, **509(31)**, 8105–8110.

47. Narayanan R. and El-Sayed M. A. (2005) Catalysis with transition metal nanoparticles in colloidal solution: nanoparticle shape dependence and stability, *J. Phys. Chem.*, **109**, 12663–12676.

48. Chithambararaj. A. and Bose, A. C. (2011) Investigation on structural, thermal, optical and sensing properties of meta-stable hexagonal MoO_3 nanocrystals of one dimensional structure, beilstein. *Journal of Nanotechnology*, **2(1)**, 585–592.

49. Klinbumrung, A., Thongtem, T. and Thongtem, S. (2012) Characterization of orthorhombic α-MoO_3 microplates produced by a microwave plasma process. *Journal of Nanomaterials*, Article ID 930763, **5**.

50. Chen, Y., Lu, C., Xu, L., Ma, Y., Hou, W. and Zhu, J. (2010) Singlecrystalline orthorhombic molybdenum oxide nanobelts: synthesis and photocatalytic properties. *Cryst Eng Comm.*, **12(11)**, 3740–3747.

51. Korchagin, A. I., Kuksanov, N. K., Lavrukhin, A. V., Fadeev, S. N., Salimov, R. A., Bardakhanov, S. P., Goncharov, V. B., Suknev, A. P., Paukshtis, E. A., Larina, T. V., Zaikovskii, V. I., Bogdanov, S. V. and Bal'zhinimaev, B. S. (2005) Production of silver nano-powders by electron beam evaporation. *7th International Conference on Electron Beam Technologies*, **77**, 485-491.

52. Song, L. X., Wang, M., Pn, S. Z., Yang, J., Chen, J. and Yang, J. (2011) Molybdenum oxide nanoparticles: preparation, characterization and application in heterogeneous catalysis. *J. Mater. Chem.*, **21**, 7982−7989.

53. Mdleleni, M. M., Hyeon, T. and Suslick, K. S. (1998) Sonochemical synthesis of nanostructured molybdenum sulfide. *J. Am. Chem. Soc.*, **120**, 6189−6190.

54. Maheswari, N. and Muralidharan, G. (2017) Controlled synthesis of nanostructured molybdenum oxide electrodes for high performance supercapacitor devices. *Applied surface science*, **416**.

55. Krishnaa, A. G., Ravikumar, R. V. S. S. N., Kumar, T. V., Ephraima, S. D., Ranjith, B., Pranoy, M. and Dolaa, S. (2016) Investigation and comparison of optical and raman bands of mechanically synthesised MoO_3. *Nano Powders Materials*, **3**, 54 – 63.

56. Xia, T., Li, Q., Liu, X., Meng, J. and Cao, X. (2012) Morphology-controllable synthesis and characterization of single-crystal molybdenum trioxide, *J. Phys. Chem.*, **110**, 2006−2012.

57. Jalalian, M., Farzaneh, F. and Foruzin, L. J.(2014) Synthesis, characterization and catalytic activity of molybdenum oxide nanoparticles by albumen, assisting microwave process for dehydrogenation of 1,4-dihydropyridines. *J. Clust Sci.*, DOI 10.1007/s10876-014-0730-4.

58. Alley, M. C., Scudiere, D. A., Monks, A., Czerwinski, M., Shoemaker, R. II. and Boyd, M. R.(1986) Validation of an automated microculture tetrazolium assay (MTA) to assess growth and drug sensitivity of human tumor cell lines. *Proc. Am. Assoc. Cancer Res.*, **27**, 389 .

59. Mosmann, T. (1983) Rapid colorimetric assay for cellular growth and survival: application to proliferation and cytotoxicity assays. *Journal of lmmunological Methods*, **65**, 55−63.

60. Odularu, A. T. O., Ajibade, P. A. and Mbese, J. Z. (2019) Impact of molybdenum compounds as anticancer agents bioinorganic chemistry and applications, Article ID 6416198, **9**.

61. Lopes, E., Piçarra, S. P. L., de Lencastre, H. and Aires-de-Sousa, M. (2018) Bactericidal efficacy of molybdenum oxide nanoparticles against antimicrobial-resistant pathogens. *Journal of Microbiology*, **678**.

62. Basu, P., Mukherjee, K., Khamrui, S., Mukherjee, S., Ahmed, M., Acharya, K., Banerjee, D., Nambissan, P. M. G. and Chatterjee, C. (2020) Oxygen, nitrogen co-doped molybdenum disulphide nano flowers for an excellent antifungal activity. *Mater. Adv.*, **1**, 1726−1738.

63. Qazi, I. A., Hashmi, I., Awan, M. A. and Zaidi N. U. -S. S.(2013) Synthesis of silver-doped titanium TiO_2 powder-coated surfaces and its ability to inactivate. *Pseudomonas aeruginosa* and *Bacillus subtilis*, *J. of Nanomaterial*, |Article ID 531010.